

Article

Performance Analysis of an Eductor-Based Membrane Distillation Unit

Ravi Koirala ¹, Quoc Linh Ve ², Eliza Rupakheti ¹, Kiao Inthavong ¹ and Abhijit Date ^{1,*}¹ School of Engineering, RMIT University, Melbourne, VIC 3083, Australia² Faculty of Engineering and Food Technology, University of Agriculture and Forestry, Hue University, Thua Thien Hue 530000, Vietnam

* Correspondence: abhijit.date@rmit.edu.au

Abstract: Thermal desalination technologies involve two primary processes: vapor generation from saline water, and effective recovery of the resulting condensate. Membrane distillation (MD) systems are among the emerging thermal desalination technologies which use a hydrophobic membrane to recover condensate through either direct or indirect contact (with the cooling fluid) condensation. The specific process technology (for thermal energy transfer and condensate recovery) depends on the type of MD. Direct contact membrane distillation (DCMD) and vacuum membrane distillation (VMD) are two significant MD processes, with DCMD having the advantage of direct condensation and simple design, while VMD systems have high yield through sub-atmospheric vapor generation. This work focuses on developing an eductor-based MD process incorporating the strengths of both DCMD and VMD. It is an experimental study with a water jet eductor replacing the vacuum pump and condenser in a typical VMD system for active permeate vapor transfer and condensation. Unlike the exiting VMD systems, the proposed design recovers condensate by direct contact condensation. The sub-cooled water acts as a motive flow which entrains the secondary vapor into the stream, causing mass transfer via condensation at the interface. The modified VMD was found to have achieved better flux compared to the conventional VMD system. The performance of the eductor, sensitivity to parameters, and the practicality of the technology have been analyzed.

Keywords: eductor; membrane distillation; compact design



Citation: Koirala, R.; Ve, Q.L.; Rupakheti, E.; Inthavong, K.; Date, A. Performance Analysis of an Eductor-Based Membrane Distillation Unit. *Water* **2022**, *14*, 3624. <https://doi.org/10.3390/w14223624>

Academic Editors: Marco Pellegrini, Cesare Sacconi and Alessandro Guzzini

Received: 16 October 2022

Accepted: 7 November 2022

Published: 10 November 2022

Publisher's Note: MDPI stays neutral with regard to jurisdictional claims in published maps and institutional affiliations.



Copyright: © 2022 by the authors. Licensee MDPI, Basel, Switzerland. This article is an open access article distributed under the terms and conditions of the Creative Commons Attribution (CC BY) license (<https://creativecommons.org/licenses/by/4.0/>).

1. Introduction

Although about 71% of the earth is covered by water, only 0.5% of it is in a usable freshwater form in rivers, lakes, and aquifers [1,2]. This fact of limited availability and increasing scarcity due to rapid urbanization is undeniable. Limited availability, overconsumption, and deterioration of freshwater sources are additional factors impacting this intensified shortage [3,4]. Despite the counterarguments, water recycling and freshwater production from sea water come forward as immediate remedies [5,6]. A variety of desalination technologies have been developed as effective solutions for brackish and saline water treatment. Broadly, they are classified based on the methods used, such as evaporation and condensation, filtration, and crystallization, which are actuated either by thermal, mechanical, electrical, or chemical energies from either renewable or non-renewable energy sources [7,8]. Thermal desalination (evaporation and condensation) has been one of the most preferred methods for freshwater production, with recent focus shifting towards membrane distillation (MD) (a membrane-based thermal desalination process). In comparison to pure thermal distillation, MD has higher energy efficiency and yield. The process involves separation of vapor from saline feed with porous hydrophobic membranes. Like many other desalination technologies, MD requires pre-treatment (coagulation, flocculation, clarification, filtration, etc.) [9].

The commercial and academic research on MD technologies involves membrane fabrication, module configuration, thermal energy sources, and spacer configuration. The

primary focus is on strength enhancement, increasing yield, optimizing energy consumption, and minimizing gap losses. There are different types of MD configurations that are named based on how the feed, membrane, and permeate interact. This paper focuses on the design optimization of the vacuum membrane distillation (VMD) system. The conventional VMD system uses a mechanical vacuum pump to maintain the vacuum on the permeate side while the permeate vapor is condensed around an indirect contact condenser.

This work uses an eductor for active vapor transfer and condensation in a VMD system. This work experimentally studies the possibility of using eductors to replace vacuum pumps and condensers in VMD units. Unlike existing VMD, this process performs direct contact condensation i.e., the vapour condenses in direct contact with the cooling water. This work has been performed with an aim to reduce the footprint of MD for developing a simple and compact portable desalination unit.

2. Technology and Mechanism Description

2.1. Eductor

Eductors are static mechanical devices that utilize pressure energy in a primary fluid (motive fluid) for suction and compression of a low-pressure secondary fluid. Both the primary and secondary fluid can be any combination of liquid, condensable gas, or non-condensable gas. Some other applications also use particles at the secondary fluid inlet. In an MD application, an eductor replaces the large vacuum pump and condensers for combined active vapor transfer and condensation. Water is used as the motive fluid for suction of saturated vapor from the permeate side of the desalination module.

Eductors consist of a primary nozzle, secondary fluid inlet pipe, suction chamber, mixing chamber, throat, and diffuser. Figure 1a shows the functional components of an eductor. The pressure energy in the motive fluid is converted to kinetic energy through the nozzle such that a low-pressure zone is created in the suction chamber which entrains the secondary fluid, explained within Figure 1b. The momentum transfer between the high-velocity motive fluid jet and the surrounding vapor carries forward the entrained fluid. The collapsing of vapor bubbles during direct contact condensation (DCC) at the interphase interface increases the secondary fluid-carrying capacity of the motive fluid. Condensation progresses along the axial direction of the eductor, and it has been found that the entrained vapor becomes completely condensed within the throat. The diffuser of an eductor is analogous to a compressor which discharges the low-pressure condensed secondary fluid to an elevated pressure. Both the mechanical and thermal activity within the system contribute to the performance of the eductor. The general performance of an eductor is measured by its entrainment ratio (Equation (1)) and pressure ratio (Equation (2)).

$$E_r = \frac{\dot{m}_s}{\dot{m}_p} \quad (1)$$

$$P_r = \frac{P_b - P_s}{P_i - P_s} \quad (2)$$

where E_r is the entrainment ratio, \dot{m}_s is the suction mass flow rate, \dot{m}_p is the primary (motive fluid) mass flow rate, and P_r is the pressure ratio. P_b is the back pressure that can be controlled by opening or closing a valve at the outlet of the eductor (beyond the pressure rising diffuser). P_s is the suction pressure that is experienced by the secondary fluid, and it is measured at an inlet to the suction port. P_i is the inlet pressure, i.e., the pressure at which the motive fluid (primary fluid) is supplied to the eductor.

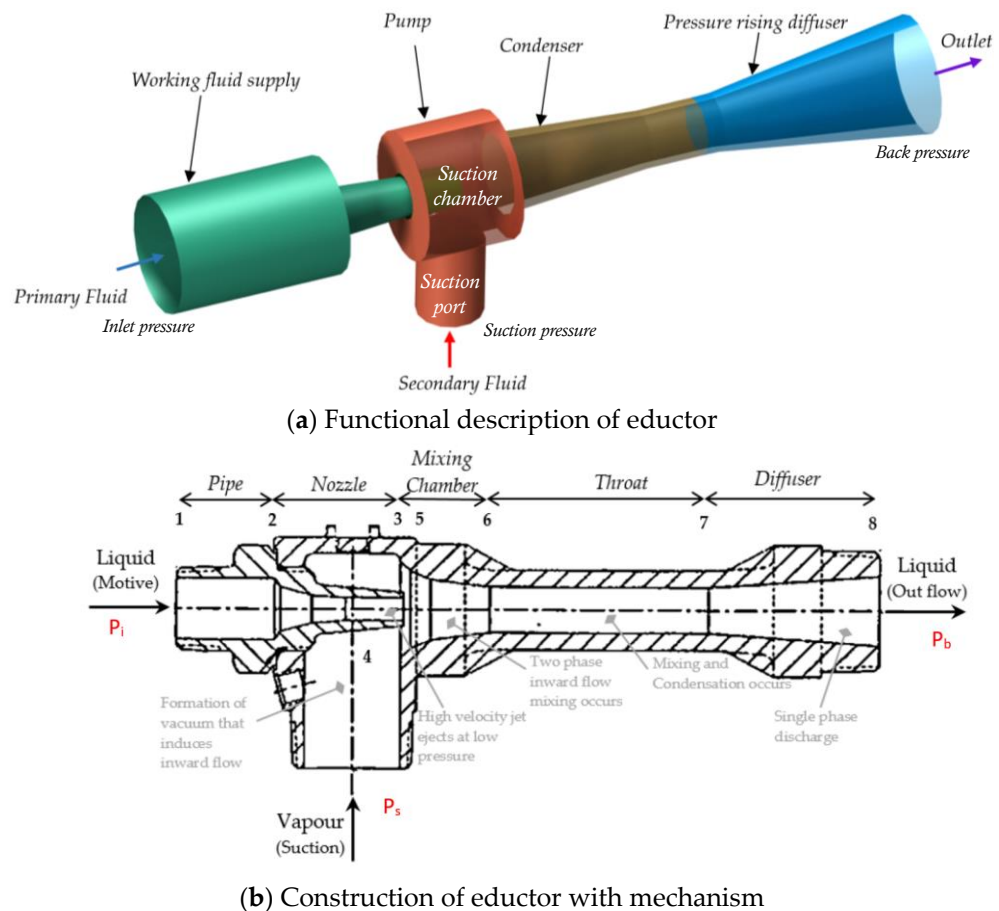


Figure 1. Components of an eductor and their function.

The entrainment of vapor into the eductor can be defined by applying an energy balance to the adiabatic secondary fluid pipe, giving the Equation (3):

$$\sqrt{2(h_{g0} - h_{g2})} - V_{g2} = 0 \tag{3}$$

where h_{g0} is the specific enthalpy of vapor at the nozzle inlet, h_{g2} is the specific enthalpy of the primary nozzle outlet, and V_{g2} is the outlet velocity of the nozzle.

For condensation based on Clausius–Clapeyron and Bernoulli’s theorem, the DCC heat transfer coefficient of vapor into a sub-cooled water jet (H_c) is defined by [10] as:

$$H_c = \frac{1.414 h_{fg}^{3/2}}{\sqrt{v_g(v_g - v_l) T_g (T_g - T_l)}} \tag{4}$$

where h_{fg} is the latent heat, v_g is the specific volume of vapor, v_l is the specific volume of liquid, T_g is the temperature of vapor, and T_l is the temperature of liquid.

The energy balance at the interface of the annular flow defines the condensation rate (dM_g/dt) within the eductor as follows [11]:

$$\frac{dM_g}{dt} = \frac{H_c (T_g - T_l) \beta}{h_{fg}} \tag{5}$$

Practically, there are two geometric points in an eductor at which choking occurs. This choking phenomenon helps in understanding the fundamental flow mechanism within the single and multiphase flow paths. It occurs when a flow passes a restriction towards a lower pressure zone at a constant mass flow rate. The first point is at the exit of the primary nozzle while the second one is in the throat. In some cases, the secondary

chocking of a two-phase flow may not be clearly observed due to the influence of outlet pressure. Koirala et al. computationally explored the entraining and condensing capacity of an eductor (Figure 2). The commercial eductor used for the work was able to achieve an entrainment ratio of 0.004, and complete condensation was achieved within the total length of 14 cm. This supports the early assumption regarding the usability of an eductor for combined vacuum generation and condensation [12]. The figure further describes the single species two-flow mechanism within an eductor. The region of interphase interaction is the zone of mass transfer, and the rate of mass transfer is higher after the throat. Similarly, complete condensation of vapor occurs within an eductor system.

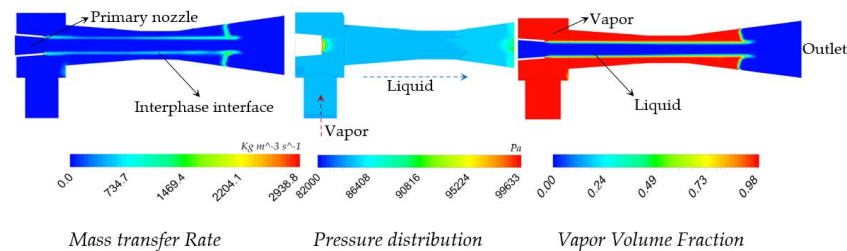


Figure 2. Two phase flow inside eductor.

2.2. Mechanism of Membrane Distillation (MD)

The condensation of permeate vapor in the primary or motive fluid (low TDS liquid water) leads to a rise in the temperature of the motive fluid which adversely effects the vacuum. It should be noted that the vacuum pressure generation capacity of an eductor is a function of the motive fluid velocity and temperature. Therefore, it is important to maintain the motive fluid flow rate above a minimum value to minimize the temperature rise of the motive fluid. In the proposed system vapor transport from the feed to the permeate side is driven by the feed temperature and vacuum pressure, like in a typical VMD system. On the other hand, the permeate vapor is condensed directly in the stream of fresh liquid water like a DCMD system and hence the proposed system could be considered as analogous to a combination of VMD and DCMD.

The thermal mechanism of freshwater production has been discussed with the aid of existing mathematical models and schematic diagram shown in Figure 3. In this section, heat and mass transfer in both direct contact membrane distillation (DCMD) and vacuum membrane distillation (VMD) are discussed. A flat plate and frame membrane module, with a flat sheet membrane, has been considered for the description of the mechanism. In both configurations (DCMD and VMD), the hot saline feedwater is pumped into the feed side where, at the feed channel, the solution directly contacts the membrane surface. The trans-membrane vapor separation mechanism and zone of condensation are two major factors differentiating the two processes. For DCMD, vapor is captured and condensed in the permeate side, where trans-membrane boundary travel is due to the vapor pressure difference resulting from the temperature difference between the two sides of the membrane. The temperature difference at the two walls is due to the boundary layer temperature of feed and permeate flows. The condensation of vapor occurs in the cold freshwater flow stream, which is pumped either counter-currently or co-currently into the permeate side of the module. For VMD, vapor is carried away from the module by the action of a vacuum pump and is condensed separately in a condenser. The transmembrane vapor travel is still due to the pressure difference, but this time it is due to vapor pressure at the feed side and the mechanically induced sub-atmospheric pressure on the permeate side. The condensation of the separated vapor occurs outside the membrane module in a specialized condenser.

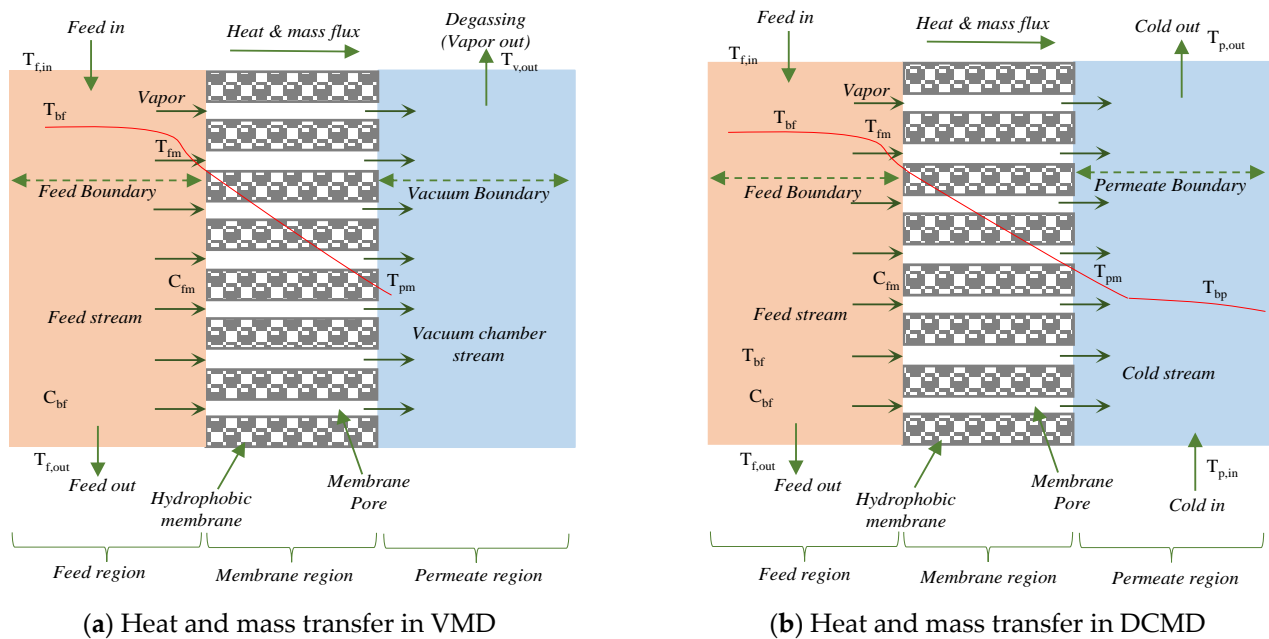


Figure 3. Heat and mass transfer in VMD and DCMD.

The DCMD process is widely used because of its simple configuration (e.g., no need for an external condenser system) and its relatively high freshwater production rate [13]. However, the low thermal energy efficiency, due to the high heat conduction losses across the membrane, is a downside for DCMD [14]. For VMD, due to the lower applied permeate pressure compared to the feed pressure of volatile vapor, which is separated from the feed solution, the vapor molecules are transferred through membrane pores from the feed to the permeate side [15]. In the case of VMD, the heat conduction losses and the heat transfer resistance on the permeate side are negligible. Therefore, higher thermal efficiency and freshwater production are expected in comparison to a DCMD module, especially at lower temperature [16]. The main drawbacks of VMD are its complicated structure and higher risk of pore wetting due to the greater pressure difference [17].

2.2.1. Heat Transfer

In membrane distillation, both heat and mass transfer occur concurrently. To acquire accurate and reliable predicted results for membrane surface temperatures and permeate flux, the dominant mechanisms of heat and mass transfer need to be determined. In general, to predict the mass transfer, the heat transfer estimation is a prerequisite [17–19]. In DCMD and VMD, convective heat transfer from the bulk feed solution through the thermal boundary layer to membrane surface on the feed side is demonstrated in Equation (6):

$$\dot{Q}_f = h_f A (T_f - T_{m,f}) \tag{6}$$

In this equation, h_f ($W \cdot m^{-2} \cdot K^{-1}$), T_f (K), and $T_{m,f}$ (K) are the convective heat transfer coefficient on the feed side, the bulk feed temperature, and the membrane surface temperature on the feed side, respectively. The bulk fluid temperature on the feed side is estimated based on the feed inlet temperature ($T_{f,in}$) and the feed outlet temperature ($T_{f,out}$) as in Equation (7):

$$T_f = \frac{T_{f,in} + T_{f,out}}{2} \tag{7}$$

The total heat transfer through the membrane consists of sensible heat (heat transferred by conduction) and latent heat (heat transferred due to the water vapor transport through membrane pores). For DCMD, this type of heat transfer can be calculated using Equation (8):

$$\dot{Q}_m = \frac{k_m}{\delta_m} A (T_{m,f} - T_{m,p}) + J_w A \Delta H_{v,w} \quad (8)$$

For VMD, the heat transfer by conduction is negligible. Therefore, Equation (8) is modified to Equation (9) [17]:

$$\dot{Q}_m = J_w A \Delta H_{v,w} \quad (9)$$

where J_w ($\text{kg}\cdot\text{m}^{-2}\cdot\text{s}^{-1}$) and $\Delta H_{v,w}$ (kJ/kg) are the permeate flux and latent heat of vaporization, respectively. $\Delta H_{v,w}$ can be evaluated at the mean membrane surface temperature T_m (K) using the Equation (10) [17,20]:

$$\Delta H_{v,w} = 1.7535T_m + 2024.3 \quad (10)$$

The thermal conductivity of the membrane can be estimated by using Maxwell's model according to Equations (11) and (12) [21]:

$$k_m = \frac{k_g \left[1 + 2\beta\varphi + (2\beta^3 - 0.1\beta)\varphi^2 + 0.05\varphi^3 \exp(4.5\beta) \right]}{1 - \beta\varphi} \quad (11)$$

$$\beta = (k_p - k_g) / (k_p + 2k_g); \varphi = 1 - \varepsilon_m \quad (12)$$

where k_g and k_p are the thermal conductivity of the gas phase inside the membrane pores and the thermal conductivity of the membrane material, respectively.

On the permeate side of a DCMD module, the heat transfer by convection from the membrane surface, through the thermal boundary layer to the bulk fluid, is given by Equation (13):

$$\dot{Q}_p = h_p A (T_{m,p} - T_p) \quad (13)$$

where h_p ($\text{W}\cdot\text{m}^{-2}\cdot\text{K}^{-1}$), T_p (K), and $T_{m,p}$ (K) are the convective heat transfer coefficient on the permeate side, bulk permeate temperature, and membrane surface temperature on the permeate side, respectively. The bulk temperature on the permeate side is estimated based on the permeate inlet temperature ($T_{p,in}$) and the permeate outlet temperature ($T_{p,out}$), and is determined using Equation (14):

$$T_p = \frac{T_{p,in} + T_{p,out}}{2} \quad (14)$$

For VMD, the convective heat transfer is not considered due to the presence of a vacuum.

In a steady state condition, the overall heat flux for a DCMD module can be derived by combining Equations (8), (10), and (14):

$$h_f A (T_f - T_{m,f}) = \frac{k_m}{\delta_m} A (T_{m,f} - T_{m,p}) + J_w A \Delta H_{v,w} = h_p A (T_{m,p} - T_p) \quad (15)$$

For a VMD module, Equation (15) can be written as shown in Equation (16):

$$h_f A (T_f - T_{m,f}) = J_w A \Delta H_{v,w} \quad (16)$$

The membrane surface temperature is calculated based on an iterative approach for energy balance in the system, defined through Equation (8).

$$T_{m,f} = \frac{h_m \left(T_p + \frac{h_f}{h_p} T_f \right) + h_f T_f - J_w \Delta H_{v,w}}{h_m + h_f \left(1 + \frac{h_m}{h_p} \right)} \quad (17)$$

$$T_{m,p} = \frac{h_m \left(T_f + \frac{h_p}{h_f} T_p \right) + h_p T_p - J_w \Delta H_{v,w}}{h_m + h_p \left(1 + \frac{h_m}{h_f} \right)} \quad (18)$$

For a VMD module, the membrane surface temperature on the feed side can be estimated based on Equation (16), as shown in Equation (19):

$$T_{m,f} = T_f - \frac{J_w \Delta H_{v,w}}{h_f} \quad (19)$$

To determine the heat transfer coefficient, the Nusselt number given by Equation (20) is appropriate. The values of Nusselt number can be estimated using the Equations (20a) and (20b) [18].

$$Nu_j = \frac{h_j d_h}{k_j} \quad (20)$$

$$Nu_j = 1.62 \times (Re Pr_d (d_h/L))^{1/3} Re < 2300 \quad (20a)$$

$$Nu_j = 0.023 \times Re^{4/5} \times Pr_d^{1/3} Re > 2300 \quad (20b)$$

where j can be for feed (f) or permeate (p), k is the solution thermal conductivity, d_h is the hydraulic diameter calculated based on spacer characteristics, L is the characteristic length, Re Reynolds number, and Pr_d Prandtl number.

2.2.2. Mass Transfer Mechanism

For DCMD, water vapor is transferred from the feed side, through the membrane pores to the permeate side, due to the vapor pressure difference, which in turn is caused by the membrane surface temperature difference. There is a relationship between mass flux (J_w) and vapor pressure difference (ΔP_v), expressed by Equation (21) [22]:

$$J_w = B_m \cdot \Delta P_v = B_m \cdot (P_{v,mf} - P_{v,mp}) \quad (21)$$

where $P_{v,mf}$ and $P_{v,mp}$ are the partial pressures of water vapor at the feed–membrane interface and permeate–membrane interface, respectively. These pressures can be estimated at $T_{m,f}$ and $T_{m,p}$ by using Sharqawy's equation [23].

In the case of VMD, the vacuum replaces the cold solution on the permeate side, therefore the partial vapor pressure at the membrane surface on the permeate side ($P_{v,mp}$) in Equation (21) can be assumed to be equal to the vacuum pressure for simplified calculation [17]. As a result, Equation (21) can be written for VMD, as showed in Equation (22):

$$J_w = B_m \cdot \Delta P_v = B_m \cdot (P_{v,mf} - P_{vacuum}) \quad (22)$$

To determine the governing mass transfer mechanism in membrane pores, the Knudsen number, as determined in Equation (23), is used:

$$Kn = \lambda_w / d_p \quad (23)$$

where the mean free path of water molecules (λ_w) can be calculated using Equation (24) [13,17].

$$\lambda_w = \frac{k_B T_m}{\sqrt{2} \pi P_m d_e^2} \quad (24)$$

where d_e , d_p , P_m , and k_B , are Collision diameters of water vapor, pore diameter, mean pressure within the membrane pores, and the Boltzman constant, respectively.

In DCMD, the viscous flow is negligible. Therefore, three types of mass transfer mechanisms in the membrane pores can be taken into consideration: molecular diffusion, combined Knudsen-molecular diffusion, and Knudsen-type diffusion [17]. In the case of VMD, the molecular diffusion is neglected, hence the viscous flow model, Knudsen flow model, and their combination are the mass transport mechanisms. Generally, the membrane distillation coefficient (B_m) for DCMD and VMD can be determined using Equations (25)–(27) as shown in Table 1 for DCMD, and Equations (28)–(30) as shown in Table 2 for VMD.

Table 1. Estimation of membrane distillation coefficient (B_m) in DCMD [17,20].

Mass Transfer Mechanism	MD Coefficient (B_m)	Eq No.	Condition
Molecular diffusion	$B_m^M = \frac{\epsilon_m}{\tau \times \delta_m} \frac{PD}{P_a} \frac{M}{RT}$	(25)	$Kn < 0.01$
Combined Knudsen-molecular diffusion	$B_m^{K-M} = \frac{1}{RT\delta_m} \left(\frac{3\tau}{2\epsilon_m r} \left(\frac{\pi M}{8RT} \right)^{1/2} + \frac{P_a \times \tau}{\epsilon_m PD} \right)^{-1}$	(26)	$0.01 < Kn < 1$
Knudsen flow model	$B_m^K = \frac{2}{3RT} \frac{\epsilon_m r}{\tau \times \delta_m} \left(\frac{8RT}{\pi M} \right)^{1/2}$ $\tau = \frac{1}{\epsilon_m}$ $PD = 1.895 \times 10^{-5} T_m^{2.072}$	(27)	$Kn > 1$

Table 2. Estimation of membrane distillation coefficient (B_m) in VMD [17].

Mass Transfer Mechanism	MD Coefficient (B_m)	Eq No.	Condition
Viscous flow model	$B_m^V = \frac{1}{RT\delta_m} \frac{\epsilon_m r^2}{8\tau\mu} p$	(28)	$Kn < 0.01$
Combined Knudsen-viscous mechanism	$B_m^{K-V} = \frac{1}{RT\delta_m} \left[\frac{2}{3} \frac{\epsilon_m r}{\tau} \left(\frac{8RT}{\pi M} \right)^{1/2} + \frac{\epsilon_m r^2}{8\tau\mu} p \right]$	(29)	$0.01 < Kn < 10$
Knudsen flow model	$B_m^K = \frac{2}{3RT} \frac{\epsilon_m r}{\tau \times \delta_m} \left(\frac{8RT}{\pi M} \right)^{1/2}$	(30)	$Kn > 10$

In Tables 1 and 2, τ , δ_m , ϵ_m , r , R , μ , M , P_a , and p , are membrane tortuosity, membrane thickness, membrane porosity, mean pore size radius, gas constant, fluid viscosity, the molecular weight of water, entrapped air pressure, and average pressure in the pore, respectively. T is the absolute temperature in the pore and T_m is the average temperature across the membrane. P is the total pressure in the pore and D is the diffusion coefficient.

In the case of the feedwater being saline, the concentration polarization effect should also be considered in the prediction of mass flux in both DCMD and VMD. During the saline water treatment process by DCMD and VMD, the concentration of bulk feed solution is lower than the concentration of the solution at the membrane surface due to the accumulation of non-volatile substances [24,25]. The relationship between mass flux and the concentration polarization coefficient (CPC) is demonstrated through implementing thin film theory, as shown in Equation (31) [17]:

$$CPC = \frac{C_{m,f}}{C_f} = \exp\left(\frac{J_w}{\rho_f k_s}\right) \tag{31}$$

where C_f , $C_{m,f}$, ρ_f , and k_s are the bulk solution concentration, solution concentration at the membrane surface, solution density, and mass transfer coefficient respectively. To determine the mass transfer coefficient, the Sherwood number correlation is used, as shown in Equation (32) [17]:

$$Sh_f = \frac{k_s \cdot d_h}{D} = 0.0588 \cdot Re_f^{0.55} \cdot Sc_f^{0.33} \tag{32}$$

where D ($m^2 \cdot s^{-1}$) and Sc_f are the diffusion coefficient of the solute and the Schmidt number, which are determined in Equations (33) and (34), respectively [26]. To simplify the modelling, it is assumed that the proposed system will operate at low salinities and the effect of salinity on the diffusion coefficient will be negligible, hence the following equation of the diffusion coefficient has been used.

$$D(T_{m,f}) = (0.72598 + 0.023087 \times T_{m,f} + 0.00027657 \times T_{m,f}^2) \times 10^{-9} \tag{33}$$

$$Sc_f = \frac{\mu_f}{\rho_f D} \tag{34}$$

3. Eductor-Based Membrane Distillation

3.1. Concept Discussion

DCMD is the simplest technology among MD configurations and operates due to a partial vapor pressure difference between the feed and permeate side. The DCC of permeate vapor is the most desirable trait in this process. Similarly, in VMD, degassing clears air from the membrane pore and maintains a sufficient pressure gradient for permeate transport. Considering the drawbacks of comparatively higher specific energy consumption and lower flux in DCMD, and the complex and bulky design in VMD, a modified VMD has been proposed, as shown in Figure 4. This schematic can be taken as a reference for developing an eductor-based water desalination unit. The setup consists of a membrane module (specifications shown in Table 3) and a commercial eductor. The saline water is recirculated in the feed side from an electric urn (simulating a generalized heat source). The permeate side of the module is a vacuum chamber, connected to the suction port of an eductor. The second freshwater loop entrains permeate vapor into the water stream, where it condenses through direct contact with the circulating liquid. The condensed permeate is then collected in an overflow tank. By incorporating the benefit of a permeate vacuum chamber and DCC, a very simple and compact water desalination unit can be developed. This system also enables effective utilization of low temperature feedwater as there is a larger potential of sub-atmospheric vapor generation.

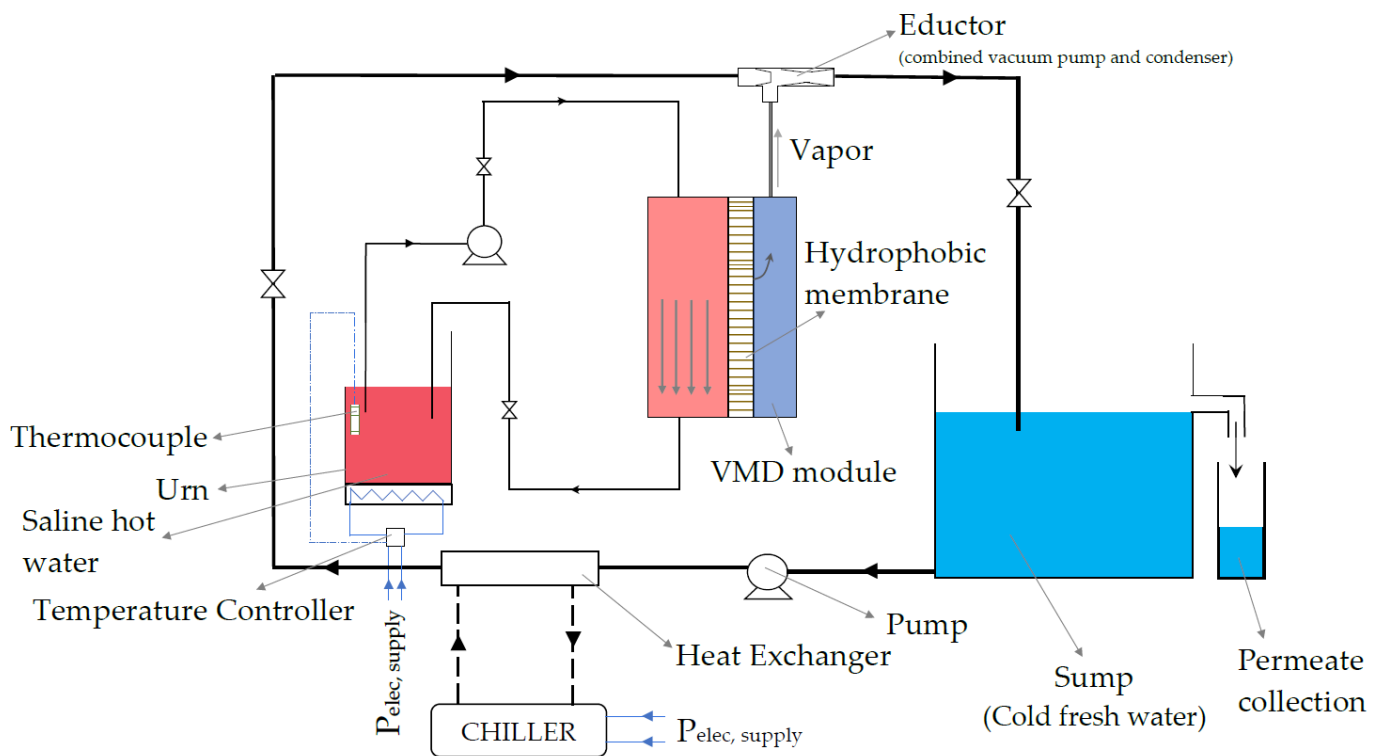


Figure 4. Eductor-based membrane distillation unit.

3.2. Experimental Set-Up Description

Figure 5 shows the experimental setup developed in the lab for this performance study. Pressure sensors and thermocouples were installed at different positions on the eductor and membrane module. The inlet, outlet, and suction pressures and temperatures were monitored for the eductor. Similarly, feed in and out flow rates and temperatures were monitored in the membrane module. The concentration of the freshwater loop is constantly monitored to ensure the functional performance of the membrane. A DataTaker DT80 data logger was used for data monitoring and acquisition. The pressures were measured through piezo-resistive transducers, temperatures were measured with k-type thermocouples, and

flow rates were measured with an ultrasonic flow meter (for feed inlet) and a vortex flow meter (for the eductor inlet).

Table 3. Physical properties of membrane module, membrane, and eductor.

Particular	Description	Units	Symbols
Membrane Module			
Width	2	mm	W
Length	180	mm	L
Breadth	180	mm	B
Membrane			
Material	PTFE		
Pore size	0.22	μm	d_p
Thickness	190–240	μm	δt
Porosity	80	%	
Eductor			
Inlet diameter	12	mm	$D_{\text{ed,in}}$
Outlet diameter	12	mm	$D_{\text{ed,out}}$
Suction diameter	12	mm	$D_{\text{ed,suc}}$
Eductor length	114	mm	L_{ed}

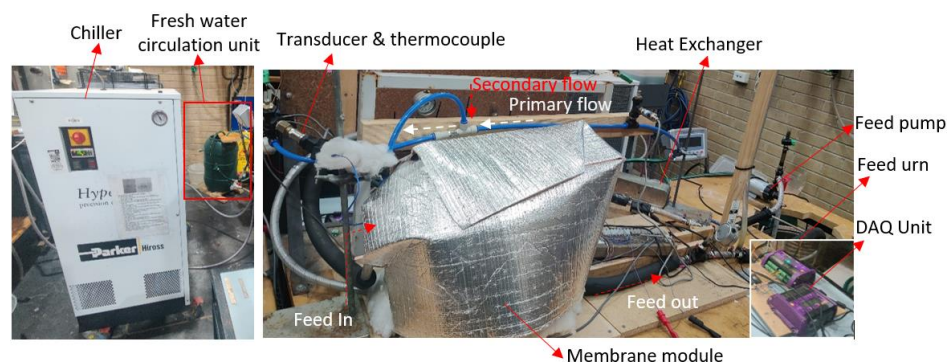


Figure 5. Experimental setup of the module.

4. Results and Discussion

The usability of an eductor for active vapor transfer and condensation in a modified VMD system has been examined in this section. It includes capacity assessment of the eductor along with the flux achieved. In addition, the thermal and electrical energy usage and sensitivity to operational parameters were examined.

4.1. Capacity Assessment of the Eductor

The concept of this membrane distillation system is based on eductor-enhanced sub-atmospheric phase separation. The assessment of the operational limit of the eductor with respect to secondary fluid pressure, P_s , has been considered as the primary factor required to plan for the operational parameters of the final water production unit.

Most of the available literature is focused on the compression of the secondary fluid to an intermediate pressure (motive > intermediate > secondary). In contrast, the ability to attain a given secondary pressure for different combinations of primary and secondary pressures has not been evaluated.

Figure 6 shows the inter-relationship between the motive fluid pressures (inlet, P_i , and outlet, P_b) and secondary fluid pressure (suction, P_s). The measurements were taken at constant inlet pressure and varying outlet pressure (also referred to as back pressure) and maintaining constant volume condition at the inlet to the suction port by closing the valve. Maintaining a constant volume condition at the suction port provided the opportunity to estimate maximum suction pressure at different back pressures (P_b). At the critical

point (choked flow), a constant P_s of 3.4 kPa (absolute) was measured for a P_b/P_i ratio of 0.27. Past this critical back pressure to inlet pressure ratio, the vacuum generation capacity of the eductor started to decrease, i.e., absolute pressure at the suction port started to increase. This continued until the P_b/P_i ratio of 0.382, where the pressure at the suction port was observed to rise above the atmospheric pressure, this indicates a flow reversal (back flow) condition where the secondary flow ceases and the motive (primary) fluid enters the suction port. Therefore, it is recommended that the proposed system be operated at sub-critical P_b/P_i ratio to ensure forward flow of the permeate from the feed to the motive fluid direction, and higher efficiency.

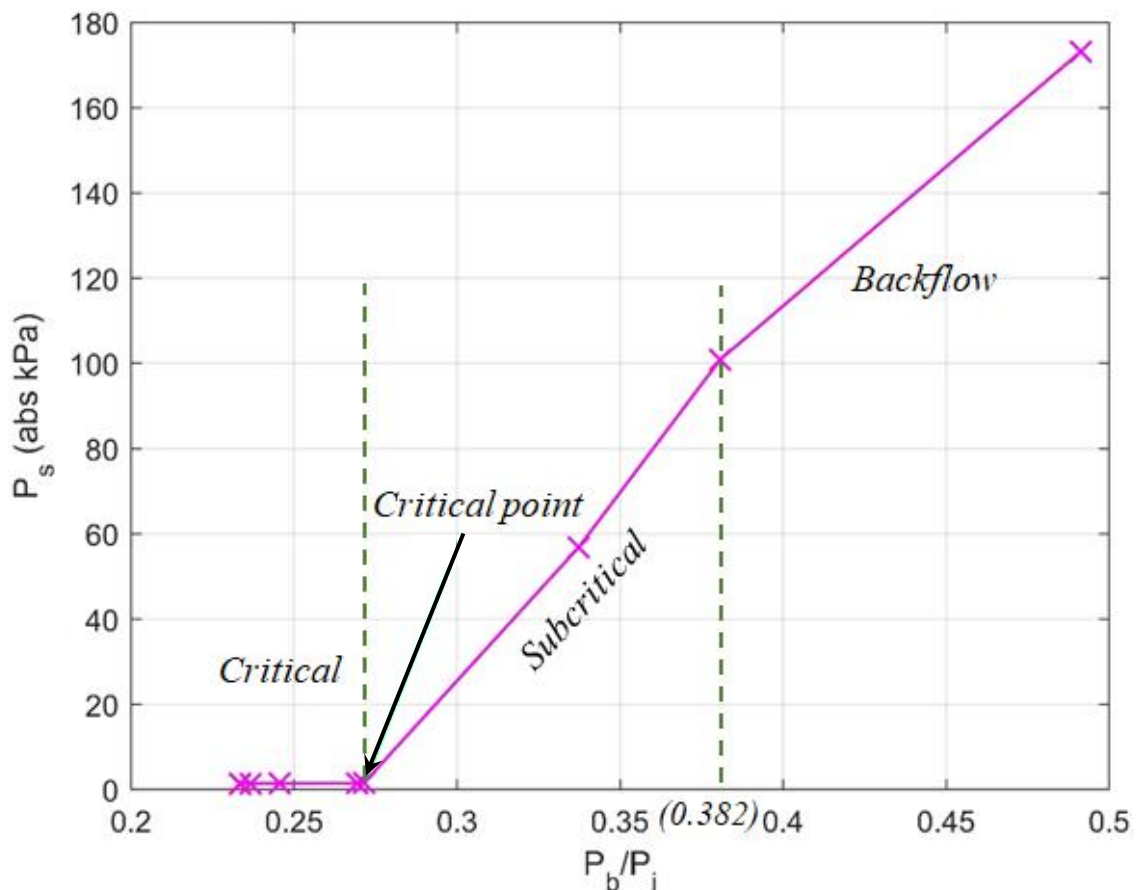


Figure 6. Experimental study of the suction capacity of an eductor.

In Figure 7, the plot for degassing duration of a vacuum sealed chamber of volume 0.0038 m^3 is shown. This aids the interpretation of the observation in Figure 6, as it provides a more descriptive depiction of the influence of P_b/P_i on the degassing rate. A piezo-resistive pressure transducer was installed in the chamber, which recorded time-dependent pressure data at a frequency of 5 Hz. The inter-relationship between back pressure and forward moving flow contributes to both momentum and thermal energy exchange within the flow path of the eductor. When the back pressure is increased at constant inlet pressure (i.e., increasing P_b/P_i), it obstructs the forward path of two-phase flow. This results in the compression of the secondary fluid until the physical limit, and eventually reduces entraining mass flow rate to cause reverse flow. Figure 6 describes the process during the compression. The average time required for complete degassing i.e., reaching a pressure of 4.2 kPa absolute, is 5.42 min.

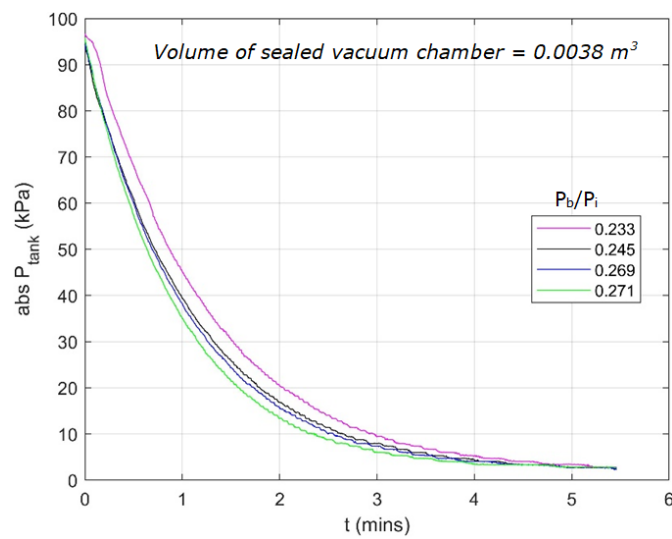


Figure 7. Degassing rate of eductor at different P_b/P_i for initialization of distillation desalination.

4.2. Performance of Desalination Module

4.2.1. Impact of Feed Temperature

The development and performance analysis of an eductor-based desalination system to replace the conventional vacuum pump and condenser in VMD is the primary focus of this work. Figure 8 shows the performance of the desalination module at four different feed temperatures (T_{fi}): 50 °C, 60 °C, 70 °C, and 80 °C. The mass flux (J) and instantaneous vacuum pressure (P_s) were plotted against P_b/P_i . The difference in operation before and after the critical point is clearly visible in all four cases, with a larger flux before the critical back pressure is reached and a sudden decline in flux after. The maximum flux for the feed temperatures of 50 °C, 60 °C, 70 °C and 80 °C are 23.1 kg·hr⁻¹·m⁻², 27.6 kg·hr⁻¹·m⁻², 33.8 kg·hr⁻¹·m⁻², and 43.12 kg·hr⁻¹·m⁻², respectively.

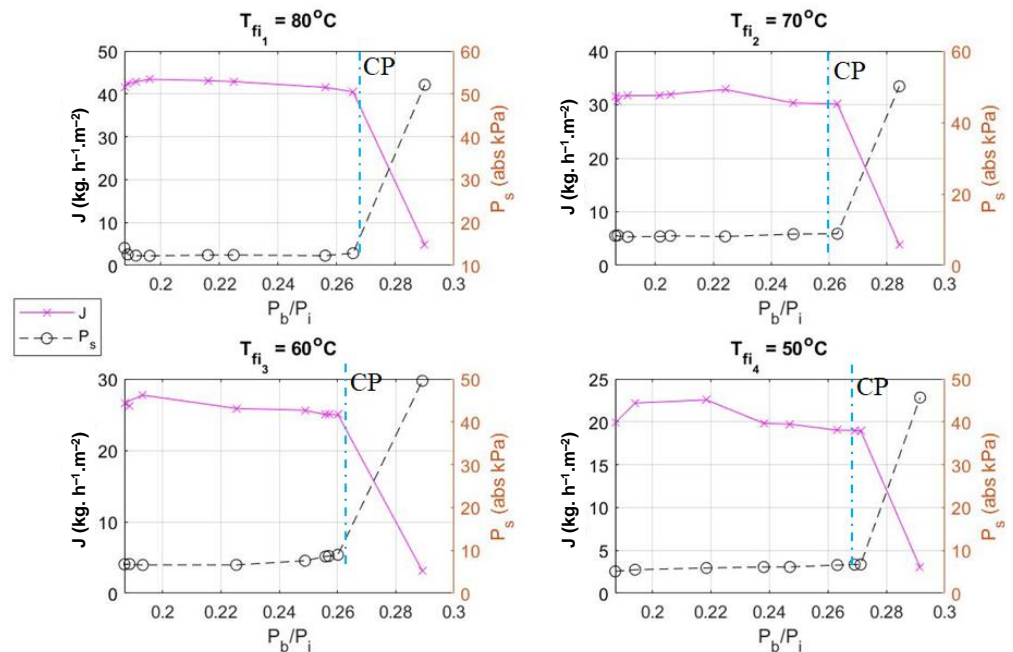


Figure 8. Mass flux (J) with respect to P_b/P_i at different T_{fi} (cold side temperature constant at $T_p = 15$ °C).

At higher temperatures, a lower latent heat of vaporization is required, hence the evaporation rate is faster. The sub-atmospheric conditions further aid this by allowing the free expansion of liquid molecules with absorption of energy. In addition to the vapor

generation, the mechanical impact (i.e., pressure propelled pumping and degassing of pores) are some of the important associated characteristics. The mechanical work can be clearly observed through the suction pressure measurements in Figures 6 and 8. This gain in the suction pressure is the influence of vapor being drawn into the system. The measurement of absolute suction pressure plotted in the secondary axis shows small variations while remaining at extreme sub-atmospheric conditions before the critical point, and a significant rise in the pressure after it. The characteristic of the eductor allows it to operate in only certain design conditions. The critical point and back flow condition depend on the design criterion considered. Increasing the back pressure beyond the critical P_b/P_i ratio results in a rapid increase in the total pressure in the suction chamber. This is due to a decrease in the velocity of the motive fluid and hence the dynamic pressure of the motive fluid in the suction chamber. This results in the observed rise in the static pressure in the suction chamber and decreases the trans-membrane pressure that drives the vapor transfer. The average absolute suction pressure at the critical points for the feed temperatures of 50 °C, 60 °C, 70 °C, and 80 °C are 7.32 kPa, 8.71 kPa, 11.52 kPa, and 13.6 kPa, respectively. Considering the utilization of mechanical energy, the region of operation around the critical point is more efficient.

4.2.2. Impact of Feedwater Flow Rate

The objective of this section is to identify the influence of feedwater flow rate (Q_{fi}) on freshwater production rate of flux (J). This relationship is shown in Figure 9. The plot is for two different feed temperatures, 70 °C and 80 °C. The observations were noted for flow rates ranging from 1 LPM to 5.2 LPM. For 80 °C, at 1.1 LPM a flux of 32.5 $\text{kg}\cdot\text{hr}^{-1}\cdot\text{m}^{-2}$ was observed, which sharply increases to 41.2 $\text{kg}\cdot\text{hr}^{-1}\cdot\text{m}^{-2}$ for a Q_{fi} of 3.18 LPM and then shows only a small variation past this point. Similarly, for the case of 70 °C, for $Q_{fi} = 1.21$ LPM, a flux of 18.1 $\text{kg}\cdot\text{hr}^{-1}\cdot\text{m}^{-2}$ was noted, which then increased sharply up to 34.5 $\text{kg}\cdot\text{hr}^{-1}\cdot\text{m}^{-2}$ for $Q_{fi} = 3.3$ LPM, and then showed only minute variations for further increases in Q_{fi} . This indicates the presence of an optimum feedwater flow rate, and shows that for operation beyond this rate, not much change in yield can be achieved. The identification of or selection of this point through design will be advantageous from both a thermal and electrical energy usage point of view. The average specific thermal energy consumption (STEC) was estimated to be around 3000 kJ/kg of permeate produced.

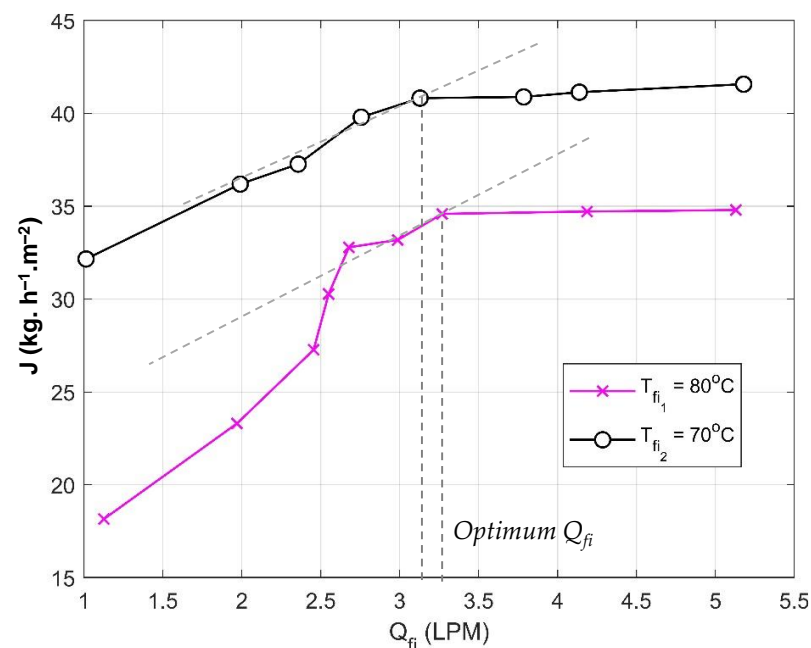


Figure 9. Mass flux (J) with respect to feed flow (Q_{fi}).

4.3. Performance of the Eductor

The initial assessment of eductors in Section 4.1 was focused on single-phase and non-condensing two-phase flows. These conditions are applicable during the start-up phase of the desalination module. In Figure 10, a more descriptive and detailed performance evaluation of an eductor for two-phase condensing flow, which includes mutual exchange of momentum, heat, and mass, is shown. The plot is for entrainment ratio (E_r) against the pressure ratio (P_r) for different temperatures of feedwater. The collective mechanical and thermal performance of the eductor can be visualized. Although the experiments were performed until reversed flow was observed, the graph only summarizes data for the conditions until critical choking occurred. The variation in P_r is a result of changes in back pressure, which indicates the compressible nature of the process.

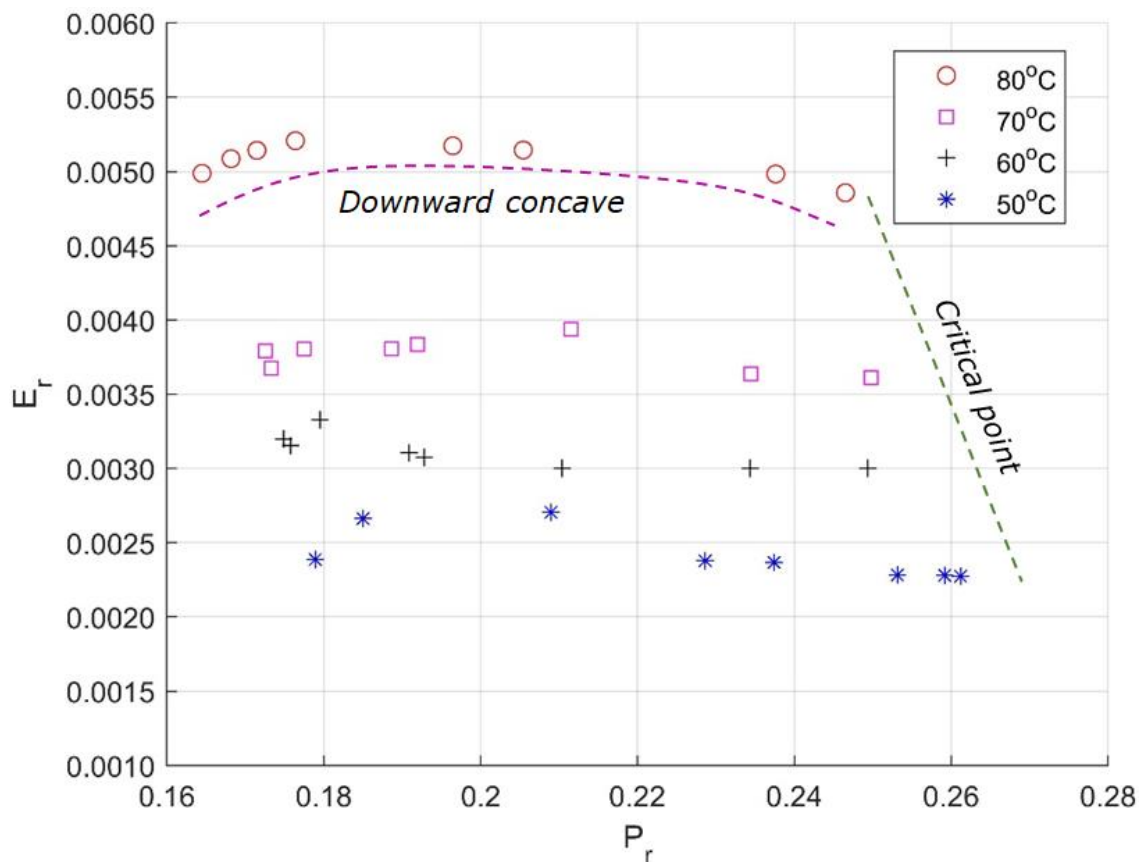


Figure 10. Performance of the eductor; entrainment ratio, E_r , vs pressure ratio, P_r .

The basic thermodynamic principles of fluid temperature and phase saturation pressure govern the trend of the increasing entrainment ratio with increasing feedwater temperature. At higher feedwater temperatures and constant sub-atmospheric pressure, the mass transfer rate is higher. With a larger proportion of vapor entraining into the flow passage, a larger proportion of momentum is shared with the low-pressure secondary fluid, resulting in earlier critical choking. Close to the critical conditions, the damping effect of the outlet pressure ensures a greater interaction time between the secondary fluid and the motive fluid, resulting in an increasing rate of condensation. Another noticeable phenomenon can be observed in the process, where with increasing back pressure, the entrainment ratio forms an asymmetric downward concave trend. Shifting of the peak E_r to the left side of the critical point is due to the combined thermal and mechanical effects on the vapor liquid interaction.

With larger bubbles collapsing, there is an increase in voids, which are then filled with more incoming vapor bubbles. The maximum E_r of 0.0053, 0.0039, 0.0034, and 0.0027 was

recorded for 80 °C, 70 °C, 60 °C, and 50 °C, respectively. The critical points for 80 °C, 70 °C, 60 °C, and 50 °C were observed at P_r of 0.244, 0.25, 0.251, and 0.262 respectively.

5. Practicality of Modified Eductor Based VMD (E-MD)

Based on the equations presented in Section 2.2.1, a theoretical study of existing VMD was performed. The model results were compared with the experimental work of Mengual et al. [27] (Figure 11) and they are in good agreement. A comparison with this experimental work has also been done by Kim et al. [28] for their theoretical study. The prime objective of this study is to establish the position of the current eductor-based membrane distillation system from the point of view of freshwater yield.

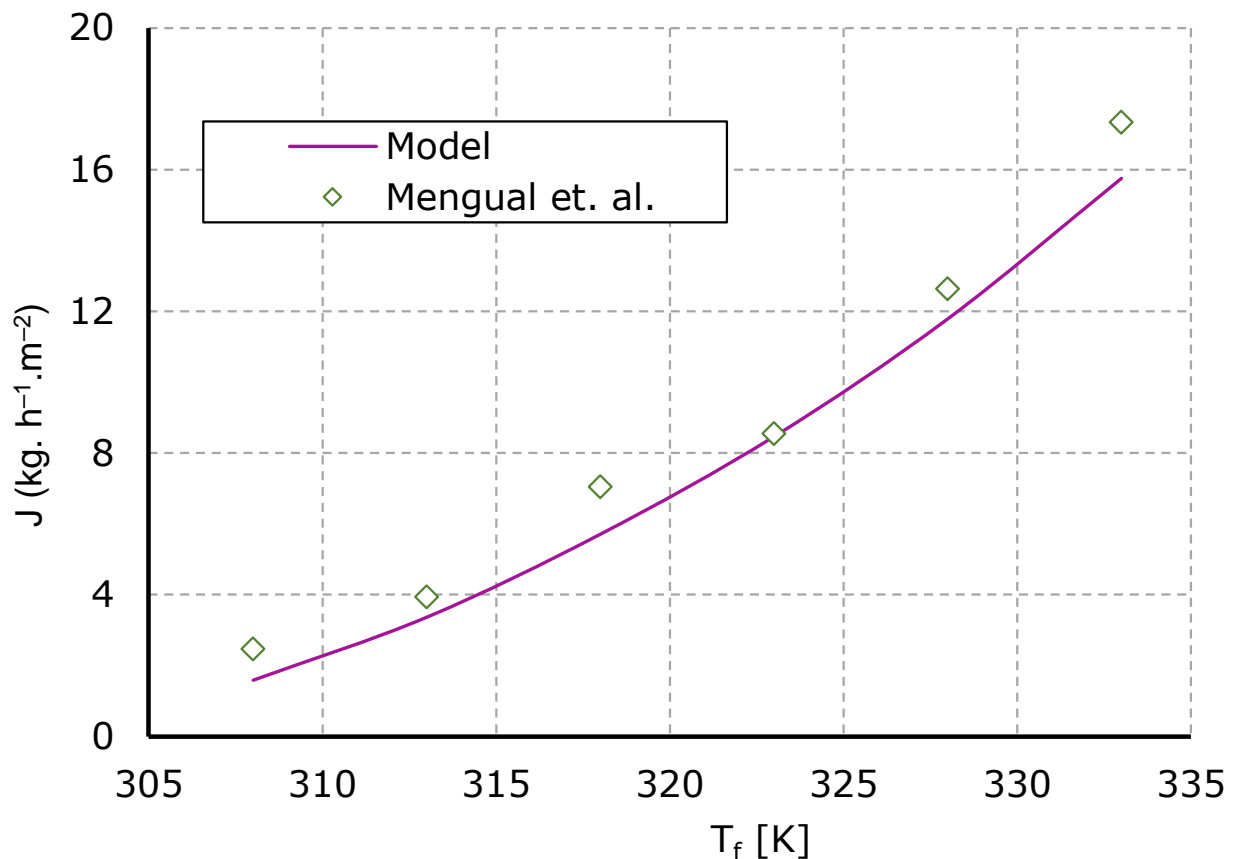


Figure 11. Validation of empirical model considered for VMD.

Figure 12 is a comparative study of the flux of the modified eductor-based VMD or E-MD with conventional VMD. The plots for VMD are based on the verified analytical model from Figure 11. The values for E-MD are selected from the maximum experimental flux at each of the recorded feedwater temperatures. The proposed eductor-based membrane distillation system, which is basically a modified VMD system, was found to have better performance compared to the model for VMD. For the feed temperature of 80 °C, the maximum flux measured experimentally was 43.1 kg·m⁻²·hr⁻¹ while for the theoretical VMD model it was 27.83 kg·m⁻²·hr⁻¹. In comparison to conventional VMD (indirect condensation), the direct contact condensation in modified VMD or E-MD is clearly more effective [29], as there is no thermal resistance at the interface like there is in a traditional condenser. This simultaneous thermal and mechanical activity of the cooling fluid in E-MD enhances the performance of the system compared to standard VMD. Although it does not use a vacuum pump, the energy consumption is relatively high compared to other technologies because of the amount of energy required for mechanical operation in the eductor.

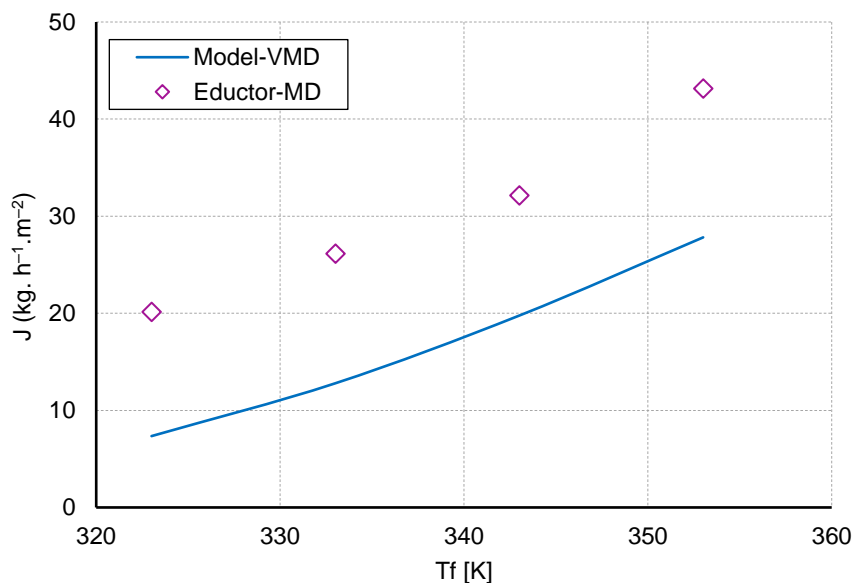


Figure 12. Flux comparison of eductor-based MD with VMD.

Figure 13 is the plot for gain output ratio (GOR) with respect to feedwater temperature (T_f). The GOR-Critical is based on the average value of flux at the critical point, and GOR-subcritical is based on the flux after the critical point. The value of GOR-Critical ranges from 0.72 to 0.87 while the value of GOR-Subcritical ranges from 0.29 to 0.31. Increasing feedwater temperature has a positive influence on the value of GOR. The value of the temperature polarization coefficient (TPC) was calculated based on the iterative process for calculating membrane surface temperature in Equations (17)–(20). The TPC was calculated to be 0.92 for 50 °C and 0.85 for 80 °C. The value of TPC decreases with increasing T_f .

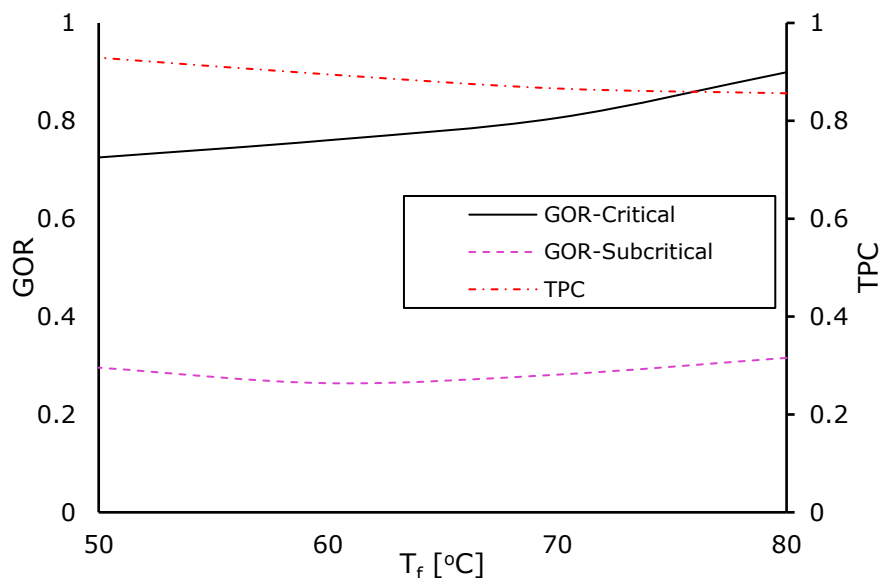


Figure 13. GOR and TPC with respect to the feed temperature.

6. Sensitivity Analysis

The use of instrumentation and control systems ensured consistent data acquisition in the experimental system. The physical parameters, such as temperature, flow rate, and pressure, were monitored using appropriate sensors. Some other influencing parameters were also monitored but were tedious to control. These parameters were identified during the experiments and were observed for the purpose of sensitivity analysis. Basically, the

temperature of eductor inlet, and rising concentration in the feedwater side are the two factors that have been discussed here.

During the mass transfer from vapor to liquid streams, the latent heat in the vapor is absorbed by motive fluid (water), the mixing that occurs as a result of turbulent flow is assumed to maintain thermal equilibrium in the motive fluid stream. The thermal energy interaction between the vapor and motive fluid stream increases the temperature of the motive fluid at the eductor outlet. If not controlled, this rise in temperature continues. The increase in T_{ei} reduces the mass transfer rate, and hence allows accumulation of vapor in the suction track, which reduces the P_r due to the increase in P_s . The experiment was conducted for about 60 min without active cooling of the motive fluid. During this experiment, T_{ei} increased from 27.6 °C to 42.1 °C. As a result, the value of P_r decreased from 0.17 to 0.162. This significantly reduced both the mechanical and thermal performance of the eductor. This experiment was conducted for $T_{fi} = 80$ °C, with the chiller turned off, and all other conditions were as per the description in Table 4. For a multiphase same-species heat transfer device like an eductor, the motive fluid temperature is an important influencing parameter that needs to be considered. In addition, the design temperature needs to be set to an easily achievable value from a work input perspective.

Table 4. Operating parameters of the hybrid system.

Particular	Description	Units	Symbols
<i>Membrane Module operating parameter</i>			
Feed flow	5.02	LPM	$Q_{f,in}$
Feed temperature	50, 60, 70 & 80 (+/-2)	°C	T_f
<i>Eductor operating parameter</i>			
Eductor inflow	4.85	LPM	$Q_{e,in}$
Eductor inlet Temperature	15	°C	$T_{e,in}$

The effect of the rise in salinity on the permeate mass flux was also observed for the salinity range of approximately 0.5% to 1% (i.e., SG of around 1.005 to 1.01). The specific gravity (SG) and flux (J) were constantly monitored during the experiment. Figure 14 is the resulting plot for J with respect to SG. The variation in J was observed to be from 39.5 kg·h⁻¹·m⁻² to 42 kg·h⁻¹·m⁻². The average experimental uncertainty of all the experiments results was around ±5.4%. The variation in the flux over the SG range of 1.005 to 1.01 was within the uncertainty and it could be said that at these low salinities, the effect of the concentration was negligible on the flux.

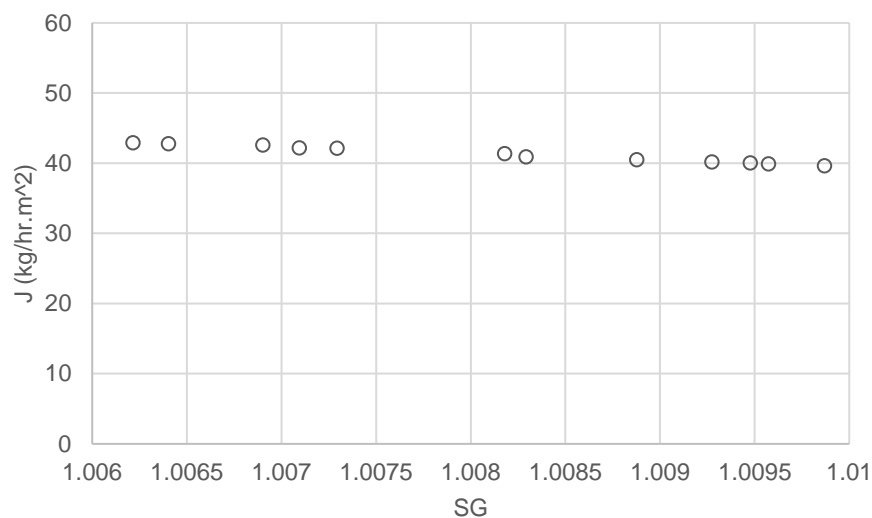


Figure 14. Influence of increasing concentration during freshwater production on flux (J).

7. Conclusions

This study was focused on developing a system using an eductor as an alternative device for active vapor transfer and condensation in a membrane distillation process. The primary activity involved a performance study of an eductor-based membrane distillation process. The proposed system incorporates the advantages of both DCMD and VMD to provide enhanced performance. A flux (J) of up to $42.9 \text{ kg}\cdot\text{h}^{-1}\cdot\text{m}^{-2}$ was calculated, which is significantly higher than conventional VMD under similar operating conditions. The value of J is dependent on Q_f , hence the optimum value is to be selected to ensure the highest energy efficiency. The operation of the eductor is segregated into critical and sub-critical regions separated by a critical point. It is always recommended to operate the eductor at the critical point.

The replacement of both the vacuum pump and condenser in VMD with an eductor will present a simple and compact technology. With no moving parts and a mechanically simple system, the adaptability and maintainability become more convenient. The E-MD system has been shown to be sensitive to motive fluid temperature in the eductor.

In summary, a simple and compact eductor-based MD system has been developed. This technology is simple, compact, and produces a greater freshwater flux compared to standard MD systems. The implementation of this technology in off-grid desalination systems will help to reduce the existing footprint of such systems. In addition, the eductor has been practically verified to be an active vapor transfer, degassing, and condensing unit. Further extending the understanding of two-phase single species flow in eductors would help in creating a simple and compact desalination system.

Author Contributions: Conceptualization, R.K. and A.D.; data curation, R.K.; formal analysis, R.K.; investigation, R.K.; methodology, R.K., A.D. and K.I.; writing—original draft, R.K.; supervision, A.D. and K.I.; writing—review and editing, R.K., Q.L.V., E.R., A.D. and K.I. All authors have read and agreed to the published version of the manuscript.

Funding: This research received no external funding.

Institutional Review Board Statement: Not applicable.

Informed Consent Statement: Not applicable.

Data Availability Statement: The data is an experimental outcome and has been stored with the first author. Data will be made available on request by sending email to ravikoirala@gmail.com.

Acknowledgments: Not applicable.

Conflicts of Interest: The authors declare no conflict of interest.

References

1. Boretti, A.; Rosa, L. Reassessing the projections of the World Water Development Report. *NPJ Clean Water* **2019**, *1*–6. [[CrossRef](#)]
2. Darre, N.C.; Toor, G.S. Desalination of Water: A Review. *Curr. Pollut. Rep.* **2018**, *4*, 104–111. [[CrossRef](#)]
3. Ibrahim, A.G.; Rashad, A.M.; Dincer, I. Exergoeconomic analysis for cost optimization of a solar distillation system. *Sol. Energy* **2017**, *151*, 22–32. [[CrossRef](#)]
4. El-Dessouky, H.; Ettouney, H. Introduction. In *Fundamentals of Salt-Water Desalination*; Elsevier Science B.V.: Amsterdam, The Netherlands, 2002.
5. Tal, A. The Desalination Debate—Lessons Learned Thus Far. *Environ. Sci. Policy Sustain. Dev.* **2011**, *53*, 34–48. [[CrossRef](#)]
6. Curto, D.; Franzitta, V.; Guercio, A. A review of the Water Desalination Technologies. *Appl. Sci.* **2021**, *11*, 670. [[CrossRef](#)]
7. Alkaisi, A.; Mossad, R.; Barforoush, A.-S. A Review of the Water Desalination Systems Integrated with Renewable Energy. *Energy Procedia* **2017**, *110*, 268–274. [[CrossRef](#)]
8. Ma, Q.; Lu, H. Wind energy technologies integrated with desalination systems: Review and state-of-the-art. *Desalination* **2011**, *277*, 274–280. [[CrossRef](#)]
9. Altmann, T.; Das, R. Process improvement of sea water reverse osmosis (SWRO) and subsequent decarbonization. *Desalination* **2021**, *499*, 114791. [[CrossRef](#)]
10. Sideman, S.; Moalem-Maron, D. Direct contact condensation. *Adv. Heat Transf.* **1982**, *15*, 227–281.
11. Zhang, Z.; Chong, D.; Yan, J. Modeling and experimental investigation on water-driven steam injector for waste heat recovery. *Appl. Therm. Eng.* **2012**, *40*, 189–197. [[CrossRef](#)]

12. Han, Y.; Wang, X.; Yuen, A.C.Y.; Li, A.; Guo, L.; Yeoh, G.H.; Tu, J. Characterization of choking flow behaviors inside steam ejectors based on the ejector refrigeration system. *Int. J. Refrig.* **2020**, *113*, 29307. [[CrossRef](#)]
13. Camacho, M.L.; Dumeé, L.; Zhang, J.; Li, J.; Duke, M.; Gomez, J.; Gray, S. Advances in membrane distillation for water de-salination and purification applications. *Water* **2013**, *5*, 94–196. [[CrossRef](#)]
14. Manawi, Y.M.; Kharaisheh, A.K.; Fard, A.K.; Benyahia, F.; Adham, S. Effect of operational parameters on distillate flux in direct contact membrane distillation (DCMD): Comparison between experimental and model predicted performance. *Desalination* **2014**, *336* (Suppl. C), 110–120. [[CrossRef](#)]
15. El-Bourawi, M.S.; Ding, A.; Ma, R.; Khayet, M. A framework for better understanding membrane distillation separation process. *J. Membr. Sci.* **2006**, *285*, 4–29. [[CrossRef](#)]
16. Koo, J.; Han, J.; Sohn, J.; Lee, S.; Hwang, T.-M. Experimental comparison of direct contact membrane distillation (DCMD) with vacuum membrane distillation (VMD). *Desalination Water Treat.* **2013**, *51*, 6299–6309. [[CrossRef](#)]
17. Khayet, M.; Matsuura, T. *Membrane Distillation: Principles and Applications*; Elsevier: Amsterdam, The Netherlands, 2011.
18. Andrjesdóttir, Ó.; Ong, C.L.; Nabavi, M.; Paredes, S.; Khalil, A.S.G.; Michel, B.; Poulikakos, D. An experimentally optimized model for heat and mass transfer in direct contact membrane distillation. *Int. J. Heat Mass Transf.* **2013**, *66*, 855–867. [[CrossRef](#)]
19. Qtaishat, M.; Matsuura, T.; Kruczek, B.; Khayet, M. Heat and mass transfer analysis in direct contact membrane distillation. *Desalination* **2008**, *219*, 272–292. [[CrossRef](#)]
20. Lawson, K.W.; Lloyd, D.R. Membrane distillation. *J. Membr. Sci.* **1997**, *124*, 1–25. [[CrossRef](#)]
21. Garcia-Payo, M.C.; Izquierdo-Gil, M.A. Thermal resistance technique for measuring the thermal conductivity of thin microporous membranes. *J. Phys. D Appl. Phys.* **2004**, *37*, 3008–3016. [[CrossRef](#)]
22. Schofield, R.W.; Fane, A.G.; Fell, C.J. Heat and mass transfer in membrane distillation. *J. Membr. Sci.* **1987**, *33*, 299–313. [[CrossRef](#)]
23. Nayar, K.G.; Sharqawy, M.H.; Banchik, L.D.; Lienhard, J.H.V. Thermophysical properties of seawater: A review and new correlations that include pressure dependence. *Desalination* **2016**, *390*, 1–24. [[CrossRef](#)]
24. Ve, Q.L.; Koirala, R.; Bawahab, M.; Faqeha, H.; Do, M.C.; Nguyen, Q.L.; Date, A.; Akbarzadeh, A. Experimental investigation of the effect of the spacer and operating conditions on mass transfer in direct contact membrane distillation. *Desalination* **2021**, *500*, 114. [[CrossRef](#)]
25. Aas, G.A.; Mea, A.; Ha, S.A.; Masa, A.M.A. Effect of different salts on mass transfer coefficient and inorganic fouling of TFC membranes. *J. Membr. Sci. Technol.* **2017**, *7*, 100175. [[CrossRef](#)]
26. Boudinar, M.B.; Hanbury, W.T.; Avlonitis, S. Numerical simulation and optimisation of spiral-wound modules. *Desalination* **1992**, *86*, 273–290. [[CrossRef](#)]
27. Mengual, J.I.; Khayet, M.; Godino, M.P. Heat and mass transfer in vacuum membrane distillation. *Int. J. Heat Mass Transf.* **2004**, *47*, 865–875. [[CrossRef](#)]
28. Kim, Y.-D.; Kim, Y.-B.; Woo, S.-Y. Detailed modeling and simulation of an out-in configuration vacuum membrane distillation process. *Water Res.* **2018**, *132*, 23–33. [[CrossRef](#)]
29. Bhuyan, D. Direct and indirect contact film-wise as well as dropwise condensation of water vapour with and without non-condensable gas-A review. *Int. Res. J. Eng. Technol.* **2020**, *7*, 10.